PCCP

Accepted Manuscript

ROYAL SOCIETY OF CHEMISTRY

www.rsc.org/pccp

Journal Name

ARTICLE TYPE

Cite this: DOI: 10.1039/xxxxxxxxxx

Extremely strong bipolar optical interactions in paired graphene nanoribbons†

Wanli Lu,*[a] Huajin Chen,[b,c] Shiyang Liu,*[b,d] Jian Zi,[b,c] and Zhifang Lin*[b,c,e]

Received Date
Accepted Date

DOI: 10.1039/xxxxxxxxxx

www.rsc.org/journalname

Graphene is an excellent multi-functional platform for electrons, photons, and phonons due to the exceptional electronic, photonic, and thermal properties. When combined its extraordinary mechanical characteristics with optical properties, the graphene-based nanostructures can serve as an appealing platform for optomechanical applications at nanoscale. Here, we demonstrate, using full-wave simulations, that there emerge extremely strong bipolar optical forces, or, optical binding and anti-binding, between a pair of coupled graphene nanoribbons, due to the remarkable confinement and enhancement of optical fields arising from the large effective mode indices. In particular, the binding and anti-binding forces, which are about two orders of magnitude stronger than that in metamaterials and high-Q resonators, can be tailored by selective excitation of either the even or the odd optical modes, achievable by tuning the relative phase of the lightwaves propagating along the two ribbons. Based on the coupled mode theory, we derive the analytical formulae for the bipolar optical forces, which agree well with the numerical results. The attractive optical binding force F_y^b and the repulsive anti-binding force F_y^a exhibit remarkable different dependence on the gap distance g between the nanoribbons and the Fermi energy E_F, in the forms of $F_y^b \propto 1/\sqrt{g^3 E_F}$ and $F_y^a \propto 1/E_F^2$. With E_F dynamically tunable by bias voltage, the bipolar forces may provide a flexible handle for active control of the nanoscale optomechanical effects, and, also, might be significant for optoelectronic and optothermal applications as well.

1 Introduction

Graphene, a single layer of carbon atoms arranged in two dimensional (2D) honeycomb lattice[1,2], has invoked comprehensive attention in recent decades due to its unique electronic, photonic, mechanical, and thermal properties. A great diversity of intriguing phenomena such as spin Hall effect for both electron[3] and photon[4], anti-Klein tunneling[5], giant Faraday rotation[6], anomalous thermoelectric transport[7], electrically tunable nonlinear effect[8], and other exotic physical consequences have been discovered in the graphene-based systems, making the graphene a promising material for various unprecedented applications in physics[9–11] and, also, in chemistry[12–15]. The latter includes, among others, surface enhanced Raman spectroscopy using graphene as a substrate[12–14], graphene based polymer composites, supercapacitors, fuel cells, sensors, and so on[15].

Among all these remarkable properties, the strong and tunable light-matter interaction mediated by graphene plasmonics exhibits increasingly magnificent prospect. Different from the surface plasmon polariton (SPP) in noble metals, the SPP in highly doped graphene arises from the collective excitation of 2D massless electron gas, showing distinctive features like relatively low loss, high confinement of optical fields, and, in particular, tunability by electric and magnetic field[9,16,17]. As a consequence, highly doped graphene is capable of serving as a superior plasmonic material in which the tunable SPP has been observed by use of low-energy electron[18,19] or near field optical microscopy[20,21]. Direct coupling of incident optical field with micro/nano graphene structures such as graphene disks[22,23], graphene rings[22], graphene holes[24], and graphene ribbons[20,21,25,26] can be achieved as well, facilitating the design of new functionalities. In addition, the atomically thin nature and the excellent electrical feature, together with its compatibility with micro/nanofabrication, mak-

[a] Department of Physics, China University of Mining and Technology, Xuzhou, Jiangsu 221116, China. E-mail: luwl@cumt.edu.cn
[b] State Key Laboratory of Surface Physics and Department of Physics, Fudan University, Shanghai 200433, China. E-mail: phlin@fudan.edu.cn
[c] Key Laboratory of Micro and Nano Photonic Structures, Fudan University, Shanghai 200433, China.
[d] Institute of Information Optics, Zhejiang Normal University, Jinhua, Zhejiang 321004, China. E-mail: syliu@zjnu.cn
[e] Collaborative Innovation Center of Advanced Microstructures, Fudan University, Shanghai 200433, China.

† Electronic Supplementary Information (ESI) available: The detailed derivations on the dispersion relation of the double-layer graphene sheets, the analytical formulae of the effective mode indices for the double-layer graphene sheets, and the analytical formulae of the optical binding and anti-binding forces for the double-layer graphene sheets. See DOI: 10.1039/b000000x/

ing graphene a good candidate for metamaterials[25,27–29], metasurfaces[30,31], and even for future optoelectronic devices compatible with the electronic integrated circuit. By far, a variety of basic optical components have been designed for plasmonics waveguide[32–35], light absorber[23,29,36–40], light polarizer[41,42], light modulator[43–45], graphene photodetector[46], and light emitting device[47], among others.

Besides, graphene also exhibits excellent mechanical features[48–50], including low mass density, great bending flexibility[51,52], and strong adhesion[53,54], which make it burgeon for the promising applications in the optomechanics[55–58], when fused with the exceptional plasmonic behaviour. A direct optical actuation for optomechanical effect yields a faster response and higher spatial resolution than the photothermal and electrostatic transductions, due to its all-optical configurations. The approach, however, requires a large optical force attainable from harvesting the linear or angular momentum carried by the photons[59–61], preferably in simple morphology. In this work, we demonstrate, by using full-wave simulations, that extremely strong bipolar optical forces can be generated between two graphene nanoribbons in the paired graphene nanoribbons (PGNRs), which is a simple and typical graphene nanostructure potentially for photonic applications[32]. Both the attractive binding and the repulsive anti-binding forces (corresponding to the even mode and the odd mode, respectively) can be observed, with fully tunable bipolar nature highly desirable for optomechanics[55–58]. The binding force F_y^b and anti-binding force F_y^a exhibit distinct features. The former is highly dependent on the separation g between two graphene nanoribbons, while the latter behaves quite insusceptibly to the change of g but strongly dependent on the Fermi energy E_F. Based on the coupling mode theory (CMT) we work out explicit analytical formulae, which agree well with the numerical results and show that F_y^b is proportional to $1/\sqrt{g^3 E_F}$, whereas F_y^a proportional to $1/E_F^2$. The dependence on E_F implies a dynamical tunability of the optical forces by the electron (or hole) doping with gate voltage, facilitating the optical manipulation of the coupled graphene ribbons and thus suggesting the possibilities of all-optical and actively tunable nanoscale optomechanical devices, and, even for optoelectronic and optothermal applications as well. Meanwhile, due to the remarkable enhancement of the electromagnetic field, strong optical gradient forces may find many applications in chemistry, such as trapping microparticles like polymers, aminoacid clusters, J-aggregates etc.[62], controlling chemical reactions within a small space by confining photopolymerization and solidication[63], and assembling polymers[64,65].

2 Results and discussion

An individual graphene nanoribbon could be treated as a plasmonic waveguide[32,33]. Compared with the traditional silicon optical waveguides or metallic plasmonic waveguides, the graphene-based plasmonic waveguides possess very large mode index, giving rise to even stronger confinement and enhancement of the optical field near the graphene sheet[16,33,66]. For a pair of graphene nanoribbons placed closely, the coupling of the plasmonic waveguide modes will induce the mode splitting, resulting in the even and odd modes[32,67]. The strong bipolar optical interactions, namely, the binding and anti-binding forces between the nanoribbons, corresponding to the even and odd modes, are demonstrated by simulations using finite-element-method (FEM) package COMSOL Multiphysics (http://www.comsol.com/). Then, the PGNRs system is solved, based on the CMT, to give the simple analytical expressions for the effective mode indices and optical forces, which agree well with the full-wave numerical results and reveal the explicit dependence of the bipolar forces on the gap distance g between ribbons and the Fermi level E_F.

2.1 Full-wave simulations based on FEM

In the theoretical framework of linear response regime, the graphene sheet is modeled as a very thin plasmonic layer with the anisotropic permittivity $\bar{\bar{\varepsilon}}$,[16,27,32]

$$\bar{\bar{\varepsilon}} = \begin{bmatrix} \varepsilon_{xx} & 0 & 0 \\ 0 & \varepsilon_{yy} & 0 \\ 0 & 0 & \varepsilon_{zz} \end{bmatrix}, \quad (1)$$

with $\varepsilon_{xx} = \varepsilon_{zz} = 2.5 + i\sigma/\varepsilon_0\omega\Delta$ and $\varepsilon_{yy} = 2.5$, where Δ is thickness of the graphene monolayer, set to be $\Delta = 0.3$ nm and compared with $\Delta = 0.5$ nm to examine the numerical convergence of the simulations, ω is the angular frequency of the optical excitations, and $\sigma = \sigma_{\text{intra}} + \sigma_{\text{inter}}$ is the conductivity of the graphene layer.

Based on the random-phase approximation at zero temperature, the conductivity contributed from intraband process σ_{intra}, with the form of Drude model, reads[34,66,68,69],

$$\sigma_{\text{intra}} = \frac{e^2 E_F}{\pi\hbar^2} \frac{i}{\omega + i\tau^{-1}}, \quad (2)$$

and that for interband process σ_{inter} can be written as,

$$\sigma_{\text{inter}} = \frac{e^2}{4\hbar}\left[\theta(\hbar\omega - 2E_F) + \frac{i}{\pi}\log\left|\frac{\hbar\omega - 2E_F}{\hbar\omega + 2E_F}\right|\right], \quad (3)$$

where $\theta(x)$ is the Heaviside step function, the Fermi energy is set as $E_F = 0.5$ eV for doped graphene, the phenomenological electron relaxation time is $\tau = 0.5$ ps, the wavelength of optical field is set as $\lambda = 8$ μm in the vacuum, corresponding to the photon energy $\hbar\omega = 0.15$ eV with $\hbar$ the reduced Planck's constant, and $-e$ is the charge of an electron. At room temperature ($T = 300$ K), the optical conductivity is still well approximated by eqns (2) and (3) for highly doped graphene ($E_F \gg k_B T$). In order to achieve graphene plasmonics with the low loss, highly doped graphene should be considered ($2E_F > \hbar\omega_{\text{Oph}}$) with $\hbar\omega_{\text{Oph}} \approx 0.2$ eV the critical optical phonon energy. For optical excitations with frequency ω satisfying the conditions $\omega < \omega_{\text{Oph}}$ and $\hbar\omega/E_F < 0.5$, the contribution of the interband electron transition to the optical conductivity σ can be neglected[68] and the phonon decay channel is closed as well.[66] With the aforementioned parameters, the real part of interband optical conductivity $\Re[\sigma_{\text{inter}}] = 0$ and the imaginary part $\frac{\Im[\sigma_{\text{inter}}]}{\Im[\sigma_{\text{intra}}]} \approx -0.01$. As a result, the optical conductivity of the highly doped graphene is solely dependent on intraband

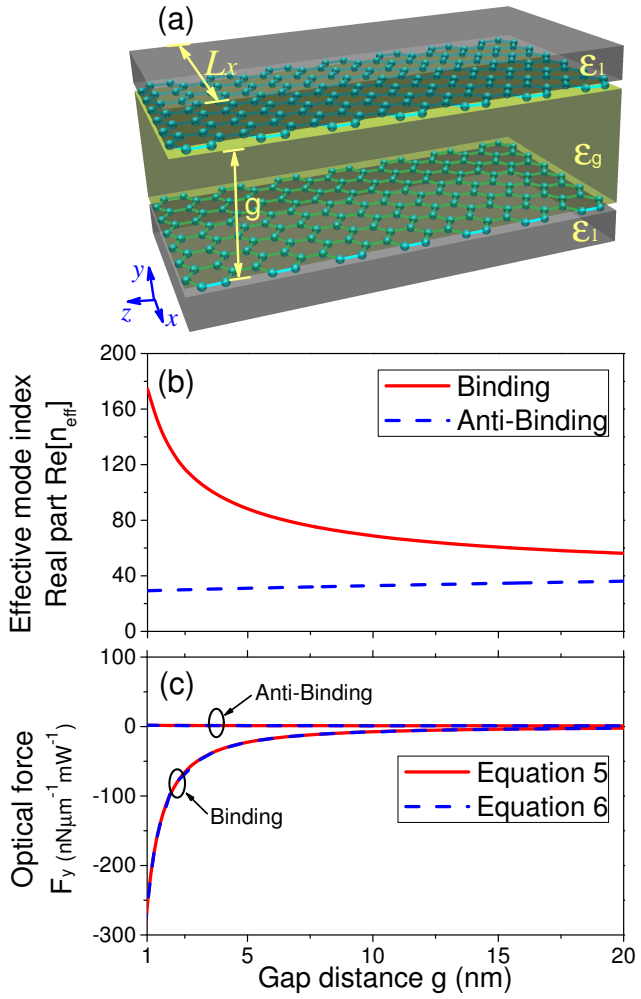

Fig. 1 (a) Schematic of the PGNRs with the width L_x and separated by the gap distance g. The effective mode indices n_{eff}^b and n_{eff}^a corresponding to the even and odd modes (b), together with the optical binding force F_y^b and anti-binding force F_y^a (c) are plotted as the functions of the gap distance g.

process and approximated by

$$\sigma \approx \sigma_{\text{intra}} = \frac{e^2 E_F}{\pi\hbar^2}\frac{i}{\omega + i\tau^{-1}}. \tag{4}$$

It should be noted that the Fermi energy E_F is given by $E_F = \hbar v_F\sqrt{\alpha\pi|V+V_0|}$, where V is the gate voltage, V_0 is the offset voltage determined by natural doping, α is a constant and v_F is the Fermi velocity[43]. Then the dynamical tunability of Fermi energy can be achieved by altering the gate voltage V, while the optical conductivity is independent of whether it is electron or hole dopping. Besides, the width of graphene nanoribbon is set to be $L_x = 25$ nm and, unlike those with the width below ~ 20 nm[70,71], the nonlocal and quantum effects could be ignored[72]. Therefore, the graphene nanoribbons considered here can be modeled as a plasmonic material with a local conductivity in classical electrodynamics. The edge termination, either armchair or zigzag edges, does not affect the results[33,72].

The PGNRs considered is schematically depicted in Fig. 1a, the bipolar optical interactions, namely, the transverse optical binding force F_y^b and anti-binding force F_y^a between two graphene nanoribbons in the PGNRs in y direction, as see in Fig. 1a, is evaluated according to the dispersion relations of the effective mode indices, for the corresponding even and odd modes. At a fixed frequency ω, it can be written as[73–75]

$$F_y = \frac{1}{c}\left.\frac{\partial\Re[n_{\text{eff}}]}{\partial g}\right|_{\omega}, \tag{5}$$

where c is the light speed in the vacuum and $\Re[n_{\text{eff}}]$ denotes the real part of the effective mode index n_{eff}. In eqn (5), F_y gives actually the optical force per unit length in z direction normalized with respect to the total power P_z propagating along z. By using the mode analysis solver of COMSOL Multiphysics, the propagation constants β of the waveguide mode at a given frequency can be calculated, which yields the effective mode index in eqn (5) through $n_{\text{eff}} = \beta/k_0$, with k_0 the wave number in vacuum.

For a single graphene nanoribbon, the effective mode index is evaluated as $n_{\text{eff}} = 45 + 0.25i$, suggesting a strong field confinement near the surface[32,33]. While for the PGNRs, the propagating eigenmodes split into symmetric and antisymmetric ones with respect to $y = 0$ plane, corresponding to the even and odd modes. The effective mode indices are shown in Fig. 1b. For the even mode, the mode index n_{eff}^b dramatically increases as the gap distance g decreases, as displayed by the red solid line. It reaches $n_{\text{eff}}^b = 174 + 0.82i$ when ribbons come close to $g = 1$ nm, implying an even higher confinement of the optical field. As a result, an extremely strong attractive binding force F_y^b between the ribbons occurs, as indicated in Fig. 1c. The optical binding force F_y^b goes up to about 260 nNμm^{-1}mW^{-1}for $g = 1$ nm. Differently, the effective mode index n_{eff}^a for the odd mode exhibits very weak dependence on the gap distance g, as illustrated by the blue dashed line in Fig. 1b. In addition, n_{eff}^a is much smaller than n_{eff}^b, indicating to a relatively weak confinement of the optical field. Therefore, the repulsive optical anti-binding force F_y^a associated with the odd mode turns out to be much weaker with the magnitude around 1 nNμm^{-1}mW^{-1}and remains nearly unchanged with g.

Similar optical binding and anti-binding effects have also been reported in other systems such as the high-Q resonators,[73] metamaterials,[75,76] and hybrid plasmonic waveguides[77], while the optical interactions between two graphene nanoribbons in the PGNRs is about two orders of magnitude stronger. This extremely strong optical interaction originates from the ultrahigh effective mode index, opening up possibilities for graphene-based nanostructures to serve as a superior platform for optomechanical effects, in comparison with the conventional configurations.[55–58] Also, the strong optical interaction is related to the abrupt change of the magnetic field between the upper and lower sides of the graphene nanoribbon, as corroborated by eqn (25) and further illustrated in Fig. S4 in the Supporting Information.

The normalized transverse optical forces can also be calculated by the integral of the Maxwell's stress tensor from the first principles in classical electrodynamics[78], which means

$$F_y = \frac{\oint_s \langle\bar{\bar{\mathbf{T}}}\rangle\cdot d\mathbf{S}}{P_z}\cdot\mathbf{e}_\mathbf{y}, \tag{6}$$

where S is a surface of unit width along z enclosing either of the ribbons, and $\langle\bar{\bar{\mathbf{T}}}\rangle$ is the time-averaged Maxwell's stress tensor given by[78]

$$\langle\bar{\bar{\mathbf{T}}}\rangle = \frac{1}{2}\mathrm{Re}\left[\varepsilon_0\varepsilon\mathbf{E}\mathbf{E}^* + \mu_0\mu\mathbf{H}\mathbf{H}^* - \frac{1}{2}(\varepsilon_0\varepsilon\mathbf{E}\cdot\mathbf{E}^* + \mu_0\mu\mathbf{H}\cdot\mathbf{H}^*)\bar{\bar{\mathbf{I}}}\right], \tag{7}$$

with $\bar{\bar{\mathbf{I}}}$ the unit tensor. The optical fields are calculated again using the FEM-based package COMSOL Multiphysics. The results for binding force F_y^b and anti-binding force F_y^a are demonstrated in Fig. 1c, which are in perfect agreement with those obtained by eqn (5), corroborating the great magnitude of the bipolar optical interactions.

2.2 Analytical formulae based on CMT

Now we proceed to work out the approximate analytical formulae to depict the explicit dependence of the bipolar optical forces, F_y^b and F_y^a, on the gap distance g as well as the Fermi energy E_F. The side view of the PGNRs is shown in Fig. 2a, which defines the coordinate system. The eigenfield profiles for the x component H_x of the magnetic field, obtained by the full-wave simulations, are illustrated in Fig. 2b and c for the even and odd modes, respectively. The near independence of H_x on the coordinate x suggests that it can be approximated by

$$H_x = \begin{cases} H_1 \exp\left[\alpha_1\left(y+\frac{g}{2}\right)\right]\exp(i\beta z), & -y > g/2, \\ \left(H_a\cosh\alpha_g y + H_b\sinh\alpha_g y\right)\exp(i\beta z), & |y| \le g/2, \\ H_2\exp\left[-\alpha_1\left(y-\frac{g}{2}\right)\right]\exp(i\beta z), & y > g/2, \end{cases} \tag{8}$$

where β is the z component of wavevector, $k_0 = \omega/c$ is the wave number in the vacuum, and ε_1 and ε_g are, respectively, the relative permittivities of the background medium and the medium between two graphene nanoribbons. The transverse components of the wave vectors are determined by $\alpha_1^2 = \beta^2 - \varepsilon_1 k_0^2$ and $\alpha_g^2 = \beta^2 - \varepsilon_g k_0^2$. The time dependence $\exp(-i\omega t)$ is assumed and suppressed. By matching the boundary conditions, the dispersion relation of the system can be obtained[67]

$$\begin{cases} \tanh\left(\frac{\alpha_g g}{2}\right) = -\frac{1}{\Gamma}, & \text{even mode}, \\ \tanh\left(\frac{\alpha_g g}{2}\right) = -\Gamma, & \text{odd mode}, \end{cases} \tag{9}$$

with

$$\Gamma = \frac{\alpha_g\varepsilon_1}{\alpha_1\varepsilon_g}\left(1 + i\frac{\alpha_1\sigma}{\varepsilon_0\varepsilon_1\omega}\right). \tag{10}$$

The propagation constants β associated with both the even and odd modes are governed by eqn (9). For the air background, $\varepsilon_1 = \varepsilon_g = 1$ and $\alpha_g = \alpha_1$, it can be simplified to retrieve the effective mode indices for both the even and odd modes in terms of $n_{\mathrm{eff}} = \beta/k_0$. With the approximations $\Re[\alpha_1]g/2 \ll 1$ and $\omega\tau \gg 1$, the real parts of the effective mode indices corresponding to the even and odd modes turn out to be

$$\begin{cases} \Re\left[n_{\mathrm{eff}}^b\right] \approx \sqrt{C_1^2/g + C_0^2} + C_0, & \text{even mode}, \\ \Re\left[n_{\mathrm{eff}}^a\right] \approx \dfrac{2C_0}{1 - C_0 k_0 g}, & \text{odd mode}, \end{cases} \tag{11}$$

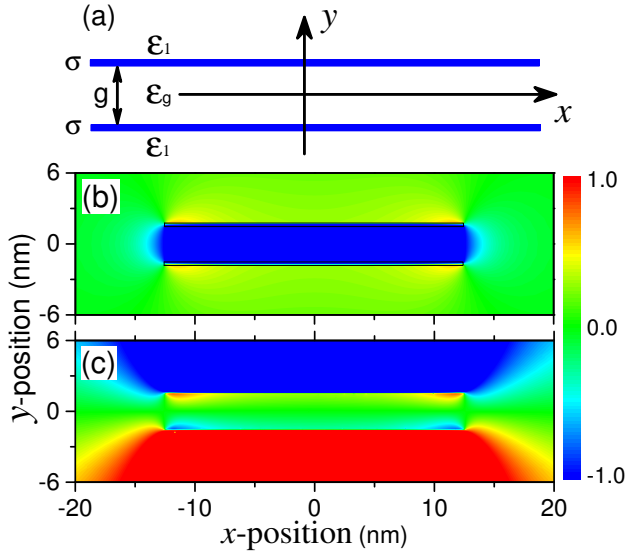

Fig. 2 (a) The side view of the PGNRs system. The eigenfield profiles of the x component of the magnetic field corresponding to the even mode H_x^b (b) and the odd mode H_x^a (c) for the case with the gap distance $g = 3$ nm.

where $C_1 = \sqrt{2\pi/\mu_0}\hbar/e\sqrt{E_F}$ and $C_0 = C_1^2 k_0/4 = \pi\hbar^2\omega/2Z_0e^2E_F$ with $Z_0 = \sqrt{\mu_0/\varepsilon_0}$ being wave impedance in the vacuum. More details on derivation is elucidated in Supporting Information. Plugging in the practical parameters for the doped graphene nanoribbons, the dimensionless parameter C_0 is evaluated as $C_0 = 5.3$ at the working wavelength 8 μm and the frequency independent parameter $C_1^2 = 2.7\times10^{-5}$ m. With $C_1^2/C_0^2 g \sim 10^2 \gg 1$ and $C_0 k_0 g \ll 1$, we arrive at an even more simple dependence on the gap distance g for the effective mode indices

$$\begin{cases} \Re\left[n_{\mathrm{eff}}^b\right] \approx C_1/\sqrt{g} + C_0, & \text{even mode}, \\ \Re\left[n_{\mathrm{eff}}^a\right] \approx 2C_0, & \text{odd mode}. \end{cases} \tag{12}$$

The results for the real part of effective mode indices based on different degrees of approximation, eqns (9) and (11), are plotted versus the gap distance g in Fig. S2 of the Supporting Information, showing a perfect agreement and justifying the approximations made in deriving eqn (11) from eqn (9). In Fig. 3a, we present the real part of effective mode indices in terms of the analytical expressions given by eqn (11) and those obtained using the full-wave FEM simulations. For the even mode (binding state), the CMT-based analytical results are in good agreement with those from the simulations, except at larger gap distance g, where the discrepancy is due to the violation of the condition $L_x \gg g$ under which our approximation works well. For the odd mode (anti-binding state), the agreement seems less satisfactory, because the eigenfield changes somewhat along x, in particular, near the edges, which causes the edge effect and thus decreases the accuracy of the approximation. The approximate analytical results, however, still agree qualitatively with the FEM simulations and reflect the main characteristics of $\Re\left[n_{\mathrm{eff}}^a\right]$ for the odd mode.

With eqn (5), the analytical formulae for the bipolar optical

interactions follow the effective mode index n_{eff} retrieved from the dispersion relation. They are

$$\begin{cases} F_y^b \approx -\dfrac{C_1}{2cg^{3/2}} \propto -\dfrac{1}{g^{3/2}\sqrt{E_F}}, & \text{even mode,} \\ F_y^a \approx \dfrac{2C_0^2 k_0}{c} \propto \dfrac{1}{E_F^2}, & \text{odd mode,} \end{cases} \tag{13}$$

where use has been made of $C_1^2/C_0^2 g \sim 10^2 \gg 1$ and $C_0 k_0 g \ll 1$. The bipolar optical interactions manifest themselves as attractive binding and repulsive anti-binding forces, associated with the even and odd modes, respectively. Their explicit dependence on the gap distance g and the Fermi energy E_F is illustrated. Substituting eqn (12) into eqn (13) yields the relations between the optical forces and the effective mode indices

$$\begin{cases} F_y^b \approx -\dfrac{\Re\left[n_{\text{eff}}^b\right]}{2cg}\left(1-\dfrac{C_0}{\Re\left[n_{\text{eff}}^b\right]-C_0}\right) \\ \quad\approx -\dfrac{\Re\left[n_{\text{eff}}^b\right]}{2cg}, & \text{even mode,} \\ F_y^a \approx \dfrac{k_0}{2c}\left(\Re\left[n_{\text{eff}}^a\right]\right)^2, & \text{odd mode,} \end{cases} \tag{14}$$

where use has been made of $\Re\left[n_{\text{eff}}^b\right] \gg C_0$ for the strongly coupled even mode.

The optical interaction between two graphene nanoribbons in the PGNRs can also be calculated by employing the integral of the Maxwell's stress tensor. Based on eqn (6) and with the fields obtained by the CMT, the optical binding and anti-binding forces for the air background medium can be worked out to be

$$\begin{cases} F_y^b = -\dfrac{\left(|\beta|^2-k_0^2\right)\Re[\alpha_1]\Im[\alpha_1]\cos\left(\Im[\alpha_1]g\right)e^{\Re[\alpha_1]g}}{\omega\Re[\beta]\left(\Im[\alpha_1^* e^{\alpha_1 g}]+\Im[\alpha_1]e^{2\Re[\alpha_1]g}\right)}, \\ F_y^a = -\dfrac{\left(|\beta|^2-k_0^2\right)\Re[\alpha_1]\Im[\alpha_1]\cos\left(\Im[\alpha_1]g\right)e^{\Re[\alpha_1]g}}{\omega\Re[\beta]\left(\Im[\alpha_1^* e^{\alpha_1 g}]-\Im[\alpha_1]e^{2\Re[\alpha_1]g}\right)}, \end{cases} \tag{15}$$

where $\Im[z]$ denotes the imaginary part of z, α_1^* is the conjugation of α_1, more details on the derivation are given in Supporting Information. Considering the facts that $\Im[\alpha_1]g \ll 1$, $k_0^2 \ll |\beta|^2$, and $\Im[\beta] \ll \Re[\beta]$, we have $\cos(\Im[\beta]g) \approx 1$ and $\sin(\Im[\alpha_1]g) \approx \Im[\alpha_1]g$ so that the optical binding and anti-binding forces can be reduced to

$$\begin{cases} F_y^b \approx -\dfrac{\Re\left[n_{\text{eff}}^b\right]}{c}\dfrac{\Re[\alpha_1]}{\Re[\alpha_1]g+\left(e^{\Re[\alpha_1]g}-1\right)}, \\ F_y^a \approx -\dfrac{\Re\left[n_{\text{eff}}^a\right]}{c}\dfrac{\Re[\alpha_1]}{\Re[\alpha_1]g-\left(e^{\Re[\alpha_1]g}+1\right)}. \end{cases} \tag{16}$$

Taking into account $\Re[\alpha_1]g \sim 0$, we have $\exp(\Re[\alpha_1]g) \approx 1+\Re[\alpha_1]g$ and two even simpler expressions can be reached

$$F_y^b \approx -\frac{\Re\left[n_{\text{eff}}^b\right]}{2cg}, \qquad \text{and} \qquad F_y^a \approx \frac{k_0}{2c}\left(\Re\left[n_{\text{eff}}^a\right]\right)^2, \tag{17}$$

which reproduce eqn (14).

For the explicit dependence of the bipolar optical forces (see eqn (13)), its validity can be further confirmed by comparing with full-wave simulations based on the FEM. The results are shown in Fig. 3b for the optical binding force associated with the even mode. An excellent agreement between the FEM simulations and our analytical expressions corroborates the explicit dependence of the attractive binding force on the gap distance g and the Fermi energy E_F. While for the optical anti-binding associated with the odd mode, a discrepancy occurs between the analytical results and the FEM simulation, as illustrated in Fig. 3c. Because the corresponding eigenfield changes somewhat with x position, especially near the edges, which results in a nonnegligible edge effect, as displayed in Fig. 2c. The neglect of the edge effect leads to an apparent underestimation of repulsive force, since the fields on the upper and lower ribbons are out of phase in the proximity of edges and thus adds significantly to the magnitude of the repulsive anti-binding force. Nonetheless, the analytical formula does reveal the weak dependence of the repulsive optical anti-binding on the gap distance g, which substantially differs from the attractive binding force.

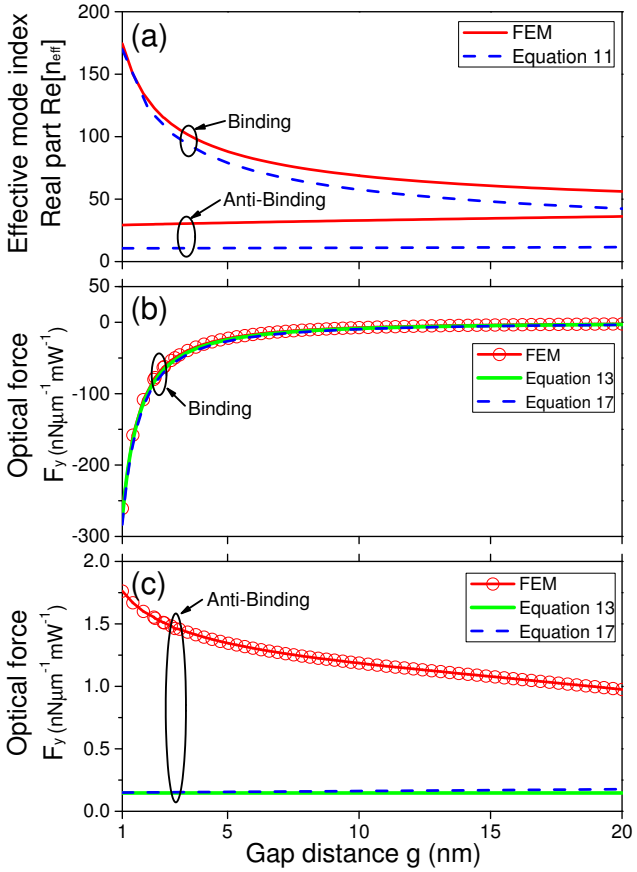

Fig. 3 (a) The effective mode indices corresponding to the even and odd modes are plotted as the functions of the gap distance g based on the full-wave FEM simulation and the analytical eqn (11). The optical binding force F_y^b (b) and anti-binding force F_y^a (c) are plotted as the functions of the gap distance g based on the full-wave FEM simulation and the analytical formulae in eqns (13) and (17).

The strong bipolar optical interactions can be observed over a relatively wide range of frequency within THz or infrared regimes. Meanwhile, the conditions $\hbar\omega/E_F \lesssim 0.5$ and $\omega < \omega_{\text{Oph}}$ are satisfied, implying that the loss due to the interband transition can be circumvented and the phonon decay channel is closed. Fig. 4 shows the effective mode indices and the optical forces

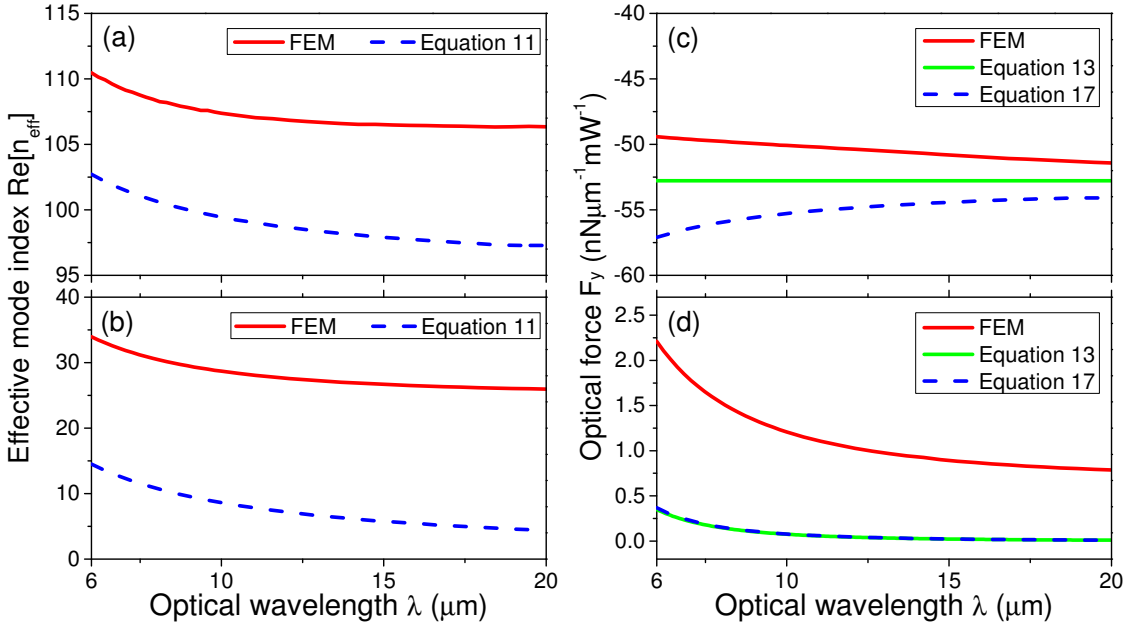

Fig. 4 The effective mode indices for the even (a) and odd (c) modes, together with the corresponding optical binding (b) and anti-binding (d) forces are plotted as the functions of the operating wavelength. Results are obtained by both numerical simulation based on the FEM and analytical expressions based on the CMT. The gap distance between two graphene nanoribbons in the PGNRs is set to be $g = 3$ nm.

as the functions of the operating wavelength λ over the range 6 μm$< \lambda <$ 20 μm. For the even mode, both the effective mode index n^b_{eff} and the optical binding force F^b_y exhibit only minor change with respect to the working wavelength, as illustrated in Fig. 4a and c, where the results obtained by numerical simulations and analytical expressions are displayed with good agreement. The insusceptibility of n^b_{eff} and F^b_y to the working wavelength straightforwardly follows from eqns (12) and (13), since C_1 is independent of the wavelength while $C_0^2 g/C_1^2 \sim 10^{-2}$ within 6 μm$< \lambda <$20 μm. The scenario is quite similar to the case for a single layer of graphene sheet suspended on a substrate in the long wavelength range.[61] For the odd mode, on the other hand, n^a_{eff} and F^a_y show non-negligible dependence on the wavelength, as indicated in Fig. 4b and d. The scaling behaviors $n^a_{\text{eff}} \sim 1/\lambda$ and $F^a_y \sim 1/\lambda^3$ are identified by the approximate analytical results, eqns (12) and 13, which roughly depict their variation with the wavelength, as compared with the full-wave simulation results, also shown in Fig. 4b and d.

As evidenced in our analytical theory, the bipolar optical interactions between two graphene nanoribbons in the PGNRs are crucially dependent on the gap distance g and the Fermi energy E_F, with the latter flexibly controllable by the gate voltage. To present an even clear picture, we present the phase diagrams with respect to g and E_F for the binding and anti-binding forces in Fig. 5. The optical binding force associated with the even mode is reminiscent of a "short range" interaction occurring only within very small gap distance g and sharply diminished with increasing the gap distance g. Differently, the optical anti-binding force associated with the odd mode behaves more like a "long range" interaction, showing small variation with the increase of the gap distance g. There is a slight deviation from the analytical theory that gives a g independent anti-binding force. The marginal dependence on

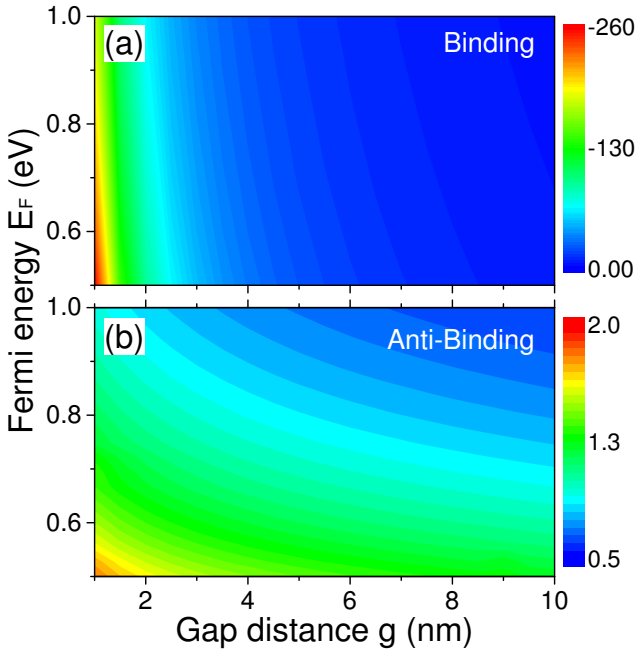

Fig. 5 Phase diagrams with respect to the Fermi energy E_F and the gap distance g for the optical binding force F^b_y (a) and the optical anti-binding force F^a_y (b) between two graphene nanoribbons in the PGNRs. The results are obtained based on the full-wave numerical simulation for ribbons with the width $L_x = 25$ nm.

g originates from the fact that the odd mode is weakly confined and thus characterized by a smaller effective mode index, as observed by comparing the field patterns shown in Fig. 2b and c. As a consequence, the odd mode exhibits nonnegligible edge effect that has not been taken into account in our analytical model, resulting in a significant underestimate of the optical force and the disagreement with the full-wave numerical simulation. Finally, although the optical binding and anti-binding force are both dependent on the Fermi energy E_F, they exhibit quite different behaviors. The optical binding force is slowly tuned, but the optical anti-binding force is sensitively tunable, thus offering more freedom in actively manipulating the graphene-based nanostructures, favorable for the implementation of tunable integrated optics, as well as nanoscale optomechanical devices.

3 Conclusions

In summary, we demonstrate in PGNRs system the emergence of extremely strong bipolar optical interactions, namely, the attractive optical binding and repulsive anti-binding forces, associated with the even and odd modes of the graphene plasmon, respectively. The bipolar optical forces possesses several distinctive features that may enable the flexible micro/nano manipulation of graphene-based systems. Firstly, the direction of the force can be reversed by excitation of either the even or the odd mode through tailoring the relative phase of the lightwaves travelling along two graphene ribbons, showing the bipolar nature just as the conventional silicon optical waveguides[79]. Secondly, the optical forces reach an unprecedented value about two orders of magnitude stronger than that in metamaterials, high-Q resonators, not to mention the conventional silicon waveguides, which originates from the abrupt change of optical field within an extremely small range due to the atomic thick nature of graphene ribbon. Thirdly, the attractive and repulsive forces show distinct dependence on the operating wavelength λ, gap distance g, and the Fermi level E_F. The dynamical controllability of the Fermi level thus enables a novel handle for tuning the optical forces on the graphene-base systems, adding considerably to the flexibility in the applications of optical manipulation, compared to the conventional optical system. These unique features, when incorporated with the exceptional mechanical properties of graphene, are expected to trigger more novel applications of graphene involved optomechanical, optoelectronic, optothermal effects, and, promisingly, for the tunable integrated optics.

Acknowledgements

This work is supported by the China 973 Projects (Grant No. 2013CB632701), MOE of China (B06011), National Natural Science Foundation of China (Grant Nos. 11574055, 11274277, 11404394, and 11574275), Zhejiang Provincial Natural Science Foundation of China (LR16A040001), the open project of SKLSP (KF2013_6) in Fudan University, and the Fundamental Research Funds for the Central Universities (2014QNA60).

References

1 K. S. Novoselov, A. K. Geim, S. V. Morozov, D. Jiang, Y. Zhang, S. V. Dubonos, I. V. Grigorieva and A. A. Firsov, *Science*, 2004, **306**, 666–669.

2 K. S. Novoselov, A. K. Geim, S. V. Morozov, D. Jiang, M. I. Katsnelson, I. V. Grigorieva, S. V. Dubonos and A. A. Firsov, *Nature*, 2005, **438**, 197–200.

3 C. L. Kane and E. J. Mele, *Phys. Rev. Lett.*, 2005, **95**, 226801.

4 A. V. Nalitov, G. Malpuech, H. Terças and D. D. Solnyshkov, *Phys. Rev. Lett.*, 2015, **114**, 026803.

5 A. Varlet, M. H. Liu, V. Krueckl, D. Bischoff, P. Simonet, K. Watanabe, T. Taniguchi, K. Richter, K. Ensslin and T. Ihn, *Phys. Rev. Lett.*, 2014, **113**, 116601.

6 I. Crassee, J. Levallois, A. L. Walter, M. Ostler, A. Bostwick, E. Rotenberg, T. Seyller, D. van der Marel and A. B. Kuzmenko, *Nat. Phys.*, 2010, **7**, 48–51.

7 P. Wei, W. Bao, Y. Pu, C. N. Lau and J. Shi, *Phys. Rev. Lett.*, 2009, **102**, 166808.

8 J. D. Cox and F. Javier García de Abajo, *Nat. Commun.*, 2014, **5**, 5725.

9 A. N. Grigorenko, M. Polini and K. S. Novoselov, *Nat. Photonics*, 2012, **6**, 749–758.

10 A. K. Geim and K. S. Novoselov, *Nat. Mater.*, 2007, **6**, 183–191.

11 F. Bonaccorso, Z. Sun, T. Hasan and A. C. Ferrari, *Nat. Photonics*, 2010, **4**, 611–622.

12 S. Huh, J. Park, Y. S. Kim, K. S. Kim, B. H. Hong and J.-M. Nam, *ACS Nano*, 2011, **5**, 9799–9806.

13 W. Xu, J. Xiao, Y. Chen, Y. Chen, X. Ling and J. Zhang, *Adv. Mater.*, 2013, **25**, 928–933.

14 X. Ling, L. Xie, Y. Fang, H. Xu, H. Zhang, J. Kong, M. S. Dresselhaus, J. Zhang and Z. Liu, *Nano Lett.*, 2010, **10**, 553–561.

15 T. Kuila, S. Bose, A. K. Mishra, P. Khanra, N. H. Kim and J. H. Lee, *Prog. Mater. Sci.*, 2012, **57**, 1061 – 1105.

16 F. H. L. Koppens, D. E. Chang and F. J. García de Abajo, *Nano Lett.*, 2011, **11**, 3370–3377.

17 F. J. García de Abajo, *ACS Photonics*, 2014, **1**, 135–152.

18 R. J. Koch, T. Seyller and J. A. Schaefer, *Phys. Rev. B*, 2010, **82**, 201413.

19 S. Y. Shin, N. D. Kim, J. G. Kim, K. S. Kim, D. Y. Noh, K. S. Kim and J. W. Chung, *Appl. Phys. Lett.*, 2011, **99**, 082110.

20 J. Chen, M. Badioli, P. Alonso-González, S. Thongrattanasiri, F. Huth, J. Osmond, M. Spasenović, A. Centeno, A. Pesquera, P. Godignon, A. Zurutuza Elorza, N. Camara, F. J. G. de Abajo, R. Hillenbrand and F. H. L. Koppens, *Nature*, 2012, **487**, 77–81.

21 Z. Fei, A. S. Rodin, G. O. Andreev, W. Bao, A. S. McLeod, M. Wagner, L. M. Zhang, Z. Zhao, M. Thiemens, G. Dominguez, M. M. Fogler, A. H. C. Neto, C. N. Lau, F. Keilmann and D. N. Basov, *Nature*, 2012, **487**, 82–85.

22 Z. Fang, S. Thongrattanasiri, A. Schlather, Z. Liu, L. Ma, Y. Wang, P. M. Ajayan, P. Nordlander, N. J. Halas and F. J. García de Abajo, *ACS Nano*, 2013, **7**, 2388–2395.

23 Z. Fang, Y. Wang, A. E. Schlather, Z. Liu, P. M. Ajayan, F. J. García de Abajo, P. Nordlander, X. Zhu and N. J. Halas, *Nano Lett.*, 2014, **14**, 299–304.

24 V. W. Brar, M. S. Jang, M. Sherrott, J. J. Lopez and H. A.

Atwater, *Nano Lett.*, 2013, **13**, 2541–2547.
25 L. Ju, B. Geng, J. Horng, C. Girit, M. Martin, Z. Hao, H. A. Bechtel, X. Liang, A. Zettl, Y. R. Shen and F. Wang, *Nat. Nanotechnol.*, 2011, **6**, 630–634.
26 H. Yan, T. Low, W. Zhu, Y. Wu, M. Freitag, X. Li, F. Guinea, P. Avouris and F. Xia, *Nat. Photonics*, 2013, **7**, 394–399.
27 A. Vakil and N. Engheta, *Science*, 2011, **332**, 1291–1294.
28 I. V. Iorsh, I. S. Mukhin, I. V. Shadrivov, P. A. Belov and Y. S. Kivshar, *Phys. Rev. B*, 2013, **87**, 075416.
29 M. A. K. Othman, C. Guclu and F. Capolino, *Opt. Express*, 2013, **21**, 7614–7632.
30 Y. Fan, N. Shen, T. Koschny and C. M. Soukoulis, *ACS Photonics*, 2014, **2**, 151–156.
31 K. Ding, S. Xiao and L. Zhou, *Front. Phys.*, 2013, **8**, 386–393.
32 J. Christensen, A. Manjavacas, S. Thongrattanasiri, F. H. L. Koppens and F. J. García de Abajo, *ACS Nano*, 2012, **6**, 431–440.
33 A. Y. Nikitin, F. Guinea, F. J. García-Vidal and L. Martín-Moreno, *Phys. Rev. B*, 2011, **84**, 161407.
34 G. W. Hanson, *J. Appl. Phys.*, 2008, **104**, 084314.
35 Y. Francescato, V. Giannini and S. A. Maier, *New J. Phys.*, 2013, **15**, 063020.
36 S. Thongrattanasiri, F. H. L. Koppens and F. J. García de Abajo, *Phys. Rev. Lett.*, 2012, **108**, 047401.
37 A. Ferreira and N. M. R. Peres, *Phys. Rev. B*, 2012, **86**, 205401.
38 T. Zhan, F. Zhao, X. Hu, X. Liu and J. Zi, *Phys. Rev. B*, 2012, **86**, 165416.
39 G. Pirruccio, L. Martín Moreno, G. Lozano and J. Gómez Rivas, *ACS Nano*, 2013, **7**, 4810–4817.
40 H. Li, Y. Anugrah, S. J. Koester and M. Li, *Appl. Phys. Lett.*, 2012, **101**, 111110.
41 Q. Bao, H. Zhang, B. Wang, Z. Ni, C. H. Y. X. Lim, Y. Wang, D. Y. Tang and K. P. Loh, *Nat. Photonics*, 2011, **5**, 411–415.
42 Y. V. Bludov, M. I. Vasilevskiy and N. M. R. Peres, *J. Appl. Phys.*, 2012, **112**, 084320.
43 M. Liu, X. Yin, E. Ulin-Avila, B. Geng, T. Zentgraf, L. Ju, F. Wang and X. Zhang, *Nature*, 2011, **474**, 64–67.
44 W. Li, B. Chen, C. Meng, W. Fang, Y. Xiao, X. Li, Z. Hu, Y. Xu, L. Tong, H. Wang, W. Liu, J. Bao and Y. R. Shen, *Nano Lett.*, 2014, **14**, 955–959.
45 E. O. Polat and C. Kocabas, *Nano Lett.*, 2013, **13**, 5851–5857.
46 F. Xia, T. Mueller, Y. Lin, A. Valdes-Garcia and P. Avouris, *Nat. Nanotechnol.*, 2009, **4**, 839–843.
47 A. Y. Nikitin, F. Guinea, F. J. Garcia-Vidal and L. Martin-Moreno, *Phys. Rev. B*, 2011, **84**, 195446.
48 X. Song, M. Oksanen, J. Li, P. J. Hakonen and M. A. Sillanpää, *Phys. Rev. Lett.*, 2014, **113**, 027404.
49 D. Akinwande, N. Petrone and J. Hone, *Nat. Commun.*, 2014, **5**, 5678.
50 C. Chen and J. Hone, *Proc. IEEE*, 2013, **101**, 1766–1779.
51 G. Tsoukleri, J. Parthenios, K. Papagelis, R. Jalil, A. C. Ferrari, A. K. Geim, K. S. Novoselov and C. Galiotis, *Small*, 2009, **5**, 2397–2402.
52 Q. Lu, M. Arroyo and R. Huang, *J. Phys. D: Appl. Phys.*, 2009, **42**, 102002.
53 S. P. Koenig, N. G. Boddeti, M. L. Dunn and J. S. Bunch, *Nat. Nanotechnol.*, 2011, **6**, 543–546.
54 J. S. Bunch and M. L. Dunn, *Solid State Commun.*, 2012, **152**, 1359–1364.
55 T. J. Kippenberg and K. J. Vahala, *Science*, 2008, **321**, 1172–1176.
56 J. Ma and M. L. Povinelli, *Curr. Opin. Solid State Mater. Sci.*, 2012, **16**, 82–90.
57 D. Van Thourhout and J. Roels, *Nat. Photonics*, 2010, **4**, 211–217.
58 M. Aspelmeyer, T. J. Kippenberg and F. Marquardt, *Rev. Mod. Phys.*, 2014, **86**, 1391–1452.
59 A. Ashkin, *Phys. Rev. Lett.*, 1970, **24**, 156–159.
60 G. S. Wiederhecker, L. Chen, A. Gondarenko and M. Lipson, *Nature*, 2009, **462**, 633–636.
61 S. H. Mousavi, P. T. Rakich and Z. Wang, *ACS Photonics*, 2014, **1**, 1107–1115.
62 S. Bartkiewicz and A. Miniewicz, *Phys. Chem. Chem. Phys.*, 2015, **17**, 1077–1083.
63 S. Ito, Y. Tanaka, H. Yoshikawa, Y. Ishibashi, H. Miyasaka and H. Masuhara, *J. Am. Chem. Soc.*, 2011, **133**, 14472–14475.
64 S. Masuo, H. Yoshikawa, H.-G. Nothofer, A. C. Grimsdale, U. Scherf, K. Mullen and H. Masuhara, *J. Phys. Chem. B*, 2005, **109**, 6917–6921.
65 T. Sugiyama, K. ichi Yuyama and H. Masuhara, *Acc. Chem. Res.*, 2012, **45**, 1946–1954.
66 M. Jablan, H. Buljan and M. Soljačić, *Phys. Rev. B*, 2009, **80**, 245435.
67 C. H. Gan, H. S. Chu and E. P. Li, *Phys. Rev. B*, 2012, **85**, 125431.
68 S. A. Mikhailov and K. Ziegler, *Phys. Rev. Lett.*, 2007, **99**, 016803.
69 B. Wunsch, T. Stauber, F. Sols and F. Guinea, *New J. Phys.*, 2006, **8**, 318.
70 C. Cocchi, D. Prezzi, A. Ruini, E. Benassi, M. J. Caldas, S. Corni and E. Molinari, *J. Phys. Chem. Lett.*, 2012, **3**, 924–929.
71 V. V. Ilyasov, B. C. Meshi, V. C. Nguyen, I. V. Ershov and D. C. Nguyen, *J. Appl. Phys.*, 2014, **115**, 053708.
72 S. Thongrattanasiri, A. Manjavacas and F. J. García de Abajo, *ACS Nano*, 2012, **6**, 1766–1775.
73 M. L. Povinelli, M. Loncar, M. Ibanescu, E. J. Smythe, S. G. Johnson, F. Capasso and J. D. Joannopoulos, *Opt. Lett.*, 2005, **30**, 3042–3044.
74 M. Povinelli, S. Johnson, M. Lonèar, M. Ibanescu, E. Smythe, F. Capasso and J. D. Joannopoulos, *Opt. Express*, 2005, **13**, 8286–8295.
75 Y. He, S. He, J. Gao and X. Yang, *Opt. Express*, 2012, **20**, 22372–22382.
76 V. Ginis, P. Tassin, C. M. Soukoulis and I. Veretennicoff, *Phys. Rev. Lett.*, 2013, **110**, 057401.
77 X. Yang, Y. Liu, R. F. Oulton, X. Yin and X. Zhang, *Nano Lett.*,

2011, **11**, 321–328.
78 J. D. Jackson, *Classical Electrodynamics*, John Wiley and Sons, New York, 3rd edn, 1999.
79 M. Li, W. H. P. Pernice and H. X. Tang, *Nat. Photonics*, 2011, **3**, 464–468.